JOURNAL OF MATERIALS SCIENCE 18 (1983) 2311–2318

On subcritical crack growth in ceramics as influenced by grain size and energy-dissipative mechanisms

A. KRELL, W. KREHER
Academy of Science of the GDR, Zentralinstitut für Festkörperphysik und Werkstofforschung, DDR-8027 Dresden, German Democratic Republic

A model is presented concerning the possibility that an unstable crack becomes stabilized by the initiation of some energy-dissipative mechanism if the stress intensity reaches a threshold value K_I^D. Depending on the toughness and the grain size distribution of the material, different crack propagation modes may occur. For sintered alumina, measurements of the fracture induced photon emission can be explained in terms of this model, substantiating in this way the assumption that microcracking is the dominating form of energy dissipation in this single phase ceramic material.

1. Introduction

Fractographic determination of the flaw size C can be used to calculate the fracture surface energy γ from the usual Griffith equation $\sigma_f = Z(2E\gamma/C)^{1/2}$, where σ_f is the fracture strength, E is Young's modulus, and Z is a geometry factor. Measuring σ_f and the initial flaw size C_0 for several polycrystalline ceramic materials Rice *et al.* [1, 2] found that the apparent fracture energy γ increases with increasing flaw size C_0 and decreasing grain size D. The effect was attributed to a transition of γ from the (lower) single crystal value γ_{sc} to γ_{pc}, the latter being characteristic for the polycrystalline material. For non-cubic materials it was shown that residual stresses can also be responsible for the variation of γ with the flaw and grain sizes [2]. In some cases the C/D-dependence of γ was also obtained by using the double cantilever beam (DCB) measuring technique.

However, Dalgleish *et al.* [3] have shown that at least for alumina such an effect might be due to the large extent of subcritical crack growth in the DCB specimens. Therefore it must be expected that the fractographic procedure too may lead to unreal variations of γ with C or D if subcritical crack growth is not taken into account, i.e. if the fracture strength is combined with the initial flaw size C_0 instead of C_f, the crack length at macroscopic instability. This point of view is supported by results of Singh *et al.* [4] who demonstrated that, having two levels of fracture energy γ_0 and γ_1 with $\gamma_1/\gamma_0 \gtrsim 5$ we generally must expect $\gamma = \gamma_1$ if subcritical crack growth occurs. Similar results have been obtained by Kirchner and Ragosta [5]. Taking into account a relation between the stress intensity K_I and the velocity of quick subcritical crack growth, they have shown that in most cases γ is determined by the polycrystalline value and that $\gamma = \gamma_{sc}$ is possible only for grain sizes exceeding 50 to 100 μm and stressing rates as high as 10^2 to 10^4 MPa sec^{-1}.

The above considerations demonstrate that subcritical crack growth has to be taken into account in order to understand the macroscopic fracture behaviour. Nevertheless, locally $\gamma = \gamma_{sc}$ will be a reasonable assumption for the onset of crack propagation at $C = C_0$ with a stress intensity K_{Ic}^0 which is considerably below the (macroscopic) critical value K_{Ic}. From a macroscopic point of view this first stage of crack propagation usually belongs to the subcritical region; on the microscale, however, a preliminary instability may occur. So the question arises whether or not the running crack can be stabilized again. Singh *et al.* [4], Virkar *et al.* [6] and Pompe *et al.* [7, 8] analysed this problem analytically assuming a local

0022–2461/83 $03.00 + .12

fracture surface energy dependent on the crack length.

In the present paper we also investigate cracks which macroscopically are propagating in the subcritical range and which may be stabilized after a first microscopic instability. In particular, we assume that stabilization may be effected by certain toughening mechanisms (especially energy dissipation by microcracking) which become active when the stress intensity K_I exceeds some threshold value K_I^D. The validity of this theoretical concept has been confirmed by certain experiments. Especially we have considered alumina ceramics where microcracking may lead to an increasing fracture toughness. In order to analyse the different stages of crack extension the fracture induced photon emission has been utilized.

2. Theory

As it is now widely accepted, a crack or flaw in a ceramic material under load may initiate the formation of an energy-dissipative zone at its tip, which under certain circumstances causes an increase in the toughness of the material. For example stress induced phase transformation in partially stabilized zirconia [9, 10] or microcracking in alumina containing ZrO_2-particles [11] may cause energy dissipation. In other polycrystalline structures without such possibilities "usual" processes as twinning, formation of river patterns, deflection of cracks at grain boundaries, and branching may also result in a critical stress intensity K_{Ic} which is higher than that of the single crystal.

Now let r_D denote the size of the zone where energy dissipation takes place (r_D is measured perpendicular to the crack plane, i.e. the distance between the outer boundaries of the zone is $2r_D$). Different theoretical considerations [12–14] have resulted in the following expression for r_D:

$$r_D = \frac{1}{3}\left(\frac{K_I}{\sigma_c}\right)^2 \qquad (1)$$

where σ_c is the critical stress at which energy dissipation starts and K_I is the applied stress intensity. The prefactor, of course, may slightly differ from 1/3 depending on the particular energy-dissipative process. Obviously, the idea of a toughness-increasing dissipation zone makes sense only if its size is larger than a certain structural length describing the distance between the dissipating elements (microcracks, transforming particles). In our case of a single phase ceramic this structural length is given by the grain size D. Therefore, an increase in toughness due to energy dissipation requires r_D to be larger than a critical value, say nD, where n depends on the particular microstructure ($n \approx 1$ to 4). Using Equation 1 we immediately arrive at a corresponding value for K_I which we denote by K_I^D:

$$K_I^D = \sigma_c(3nD)^{1/2}. \qquad (2)$$

The characteristic K_I^D acts as a threshold value for the onset of energy dissipation. Let us denote the two levels of specific fracture surface work by γ_0 and γ_1, where γ_0 is the reference value without energy dissipation and γ_1 is the governing quantity when energy dissipation takes place. Furthermore we assume a step-like change at $K_I = K_I^D$:

$$\gamma = \begin{cases} \gamma_0 & \text{for } K_I < K_I^D \\ \gamma_1 & \text{for } K_I \geqslant K_I^D \end{cases} \qquad (3)$$

This approximation seems to be appropriate in order to discuss the physical effects caused by such a transition of γ (the more complicated case of a smooth transition has been dealt with by Singh *et al.* [4] and Pompe *et al.* [7]). It is useful to define critical stress intensities K_{Ic}^0 and K_{Ic}^1 as derived from γ_0 and γ_1 by the usual relations

$$K_{Ic}^0 = (2E\gamma_0)^{1/2}, \quad K_{Ic}^1 = (2E\gamma_1)^{1/2}, \qquad (4)$$

(in this paper we shall not differentiate between plane stress and plane strain conditions, hence we neglect the difference between E and $E/(1-\nu^2)$. where ν is Poisson's ratio).

In the following we suppose $\gamma_1 > \gamma_0$, i.e. energy dissipation increases the toughness. Actually γ_0 and γ_1 depend on numerous microstructural parameters (e.g. [13]) but these dependencies will not be a subject of this paper. Rather we shall consider γ_0 and γ_1 as material properties given by theory or experiment. Starting from this position we shall investigate which of the two levels of γ determines the macroscopic fracture toughness K_{Ic}. In particular we shall consider two questions: 1. Crack propagation starts at an applied stress intensity $K_I = K_{Ic}^0 < K_I^D$. Subsequently K_I increases due to the elongation of the crack. Can the crack be stabilized again by the onset of the energy-dissipative process? 2. If we compare two ceramic microstructures having different grain size distributions, how is the threshold stress intensity K_I^D influenced by the grain sizes? Let us start with the first problem. As in [4] we make use of the

energy balance

$$-\Delta P = \Delta W_\gamma \tag{5}$$

i.e. the crack can only be arrested if the elastic energy $-\Delta P$ released during crack extension equals the fracture surface work ΔW_γ consumed in this process. Since Equation 5 neglects the possible dissipation of kinetic energy, actually it will provide an upper limit for the crack arrest length. The energy release $-\Delta P$ may be derived from the energy release rate

$$G = K_I^2/E. \tag{6}$$

The stress intensity K_I depends on the crack size C via

$$K_I = \frac{1}{Z}\sigma(C)^{1/2} \tag{7}$$

where σ is the applied stress and Z a geometry factor. Due to the exponential increase of crack velocity with K_I, even during subcritical stages we are concerned with a relatively rapid crack propagation. Therefore, we can assume that the applied stress is approximately constant during crack growth and K_I increases mainly due to the growing value of C. Then σ can be calculated from the condition $K_I = K_{Ic}^0$ at the starting length $C = C_0$. Equation 7 yields

$$\sigma = Z \cdot K_{Ic}^0/C_0^{1/2}. \tag{8}$$

Substituting for K_I in Equation 6 by the help of Equations 7, 8, and 4 gives the energy release rate at constant load dependent on the crack length C:

$$G = G(C) = 2\gamma_0 C/C_0. \tag{9}$$

The fracture surface work ΔW_γ can be immediately derived from the specific work γ of Equation 3. Since K_I depends on the crack size, the $\gamma_0 \rightarrow \gamma_1$ transition proceeds after a certain amount of crack elongation. This particular crack size, say C_D, can be calculated from Equations 7 and 8 when K_I is replaced by K_I^D:

$$C_D = C_0(K_I^D/K_{Ic}^0)^2. \tag{10}$$

Thus we have the result that for $C < C_D$ the fracture surface work is given by γ_0 whereas for $C \geqslant C_D$ it is determined by γ_1. Note that C_D is proportional to the starting length C_0, i.e. it is not a material constant.

In order to simplify the analytical procedure, let us assume that the propagation of the macrocrack is a one-dimensional process. Of course this is only an approximation, but it describes well the principal modes of crack extension which occur in reality. Therefore, the energy balance (Equation 5) may be expressed by G and γ in the following form:

$$\int_{C_0}^{C_s} G(C)\mathrm{d}C = 2\int_{C_0}^{C_s} \gamma(C)\mathrm{d}C \tag{11}$$

where C_s denotes the crack arrest length. Inserting Equation 3 and 9 into 11 yields

$$\gamma_0(C_s^2 - C_0^2)/C_0 = 2\gamma_0(C_D - C_0) + 2\gamma_1(C_s - C_D) \tag{12}$$

from which we obtain for C_s:

$$\frac{C_s}{C_0} = \frac{1}{(K_{Ic}^0)^2}\left[\!\left[(K_{Ic}^1)^2 - \{[(K_{Ic}^1)^2 - (K_{Ic}^0)^2] \times [(K_{Ic}^1)^2 + (K_{Ic}^0)^2 - 2(K_I^D)^2]\}^{1/2}\right]\!\right] \tag{13}$$

Here we have replaced γ_0 and γ_1 by K_{Ic}^0 and K_{Ic}^1 using Equation 4. From Equation 13 we observe that crack arrest is possible only if the following condition is satisfied:

$$K_I^D \leqslant \{[(K_{Ic}^0)^2 + (K_{Ic}^1)^2]/2\}^{1/2}. \tag{14}$$

Otherwise no real solution for C_s exists, i.e. the increase in toughness at K_I^D is insufficient to stabilize the running crack. Now we can summerize the different modes of crack propagation which are schematically represented in Fig. 1.

(i)

$$K_I^D \leqslant K_{Ic}^0 < K_{Ic}^1 \tag{15}$$

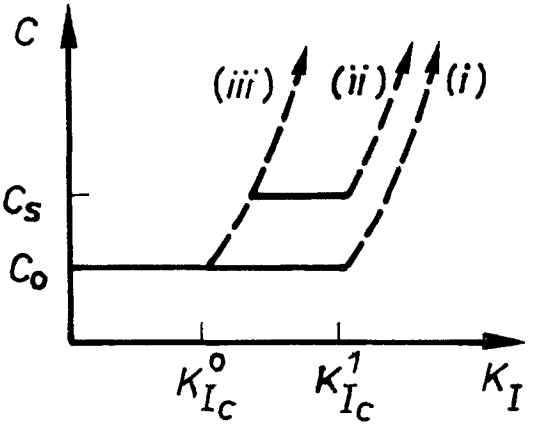

Figure 1 Relations between the crack length C and the applied stress intensity K_I. For the resting crack (solid lines) the increase of K_I is provided by the growing load whereas during unstable stages (dotted lines) K_I increases due to the crack elongation at almost constant macroscopic stress (Equation 7). See text for propagation modes (i), (ii), (iii).

The energy-dissipative zone is already active before the onset of crack propagation. Therefore, K_I must be increased beyond K_{Ic}^0 up to K_{Ic}^1 in order to initiate crack propagation. Then the crack starts from its original length C_0 and no subsequent stabilization takes place.

(ii)

$$K_{Ic}^0 < K_I^D \leqslant \{[(K_{Ic}^0)^2 + (K_{Ic}^1)^2]/2\}^{1/2} < K_{Ic}^1 \quad (16)$$

The crack becomes unstable (at least on the microscale) at K_{Ic}^0. Due to the increasing K_I, energy dissipation commences at K_I^D and the crack becomes stabilized at the length C_s given by Equation 13. Then the load must be further increased to cause final instability at K_{Ic}^1.

(iii)

$$\{[(K_{Ic}^0)^2 + (K_{Ic}^1)^2]/2\}^{1/2} < K_I^D \quad (17)$$

Here again crack propagation starts at K_{Ic}^0. Energy dissipation is initiated after a certain amount of crack elongation but, in contrast to mode (ii), it is insufficient to prevail against the energy release of the running crack and to stabilize it. Therefore, K_{Ic}^1 has no influence on this mode of crack propagation.

Now we turn to our second problem concerning the influence of the grain size D on the threshold stress intensity K_I^D (Equation 2). Here we shall concentrate on microcracking at grain boundaries since this mechanism appears to be the dominating energy-dissipative process in single phase alumina. In order to calculate σ_c, the critical local stress at which microcracking starts, we must take into account the residual stresses being inherent to most ceramics. In polycrystalline Al_2O_3 they are due to thermal expansion anisotropy. Especially the tensile residual stress σ_i is important since it reduces σ_c below that critical stress σ_{mc} which would be necessary to initiate microcracking in the absence of residual stresses:

$$\sigma_c = \sigma_{mc} - \sigma_i. \quad (18)$$

The residual stress σ_i can be assumed to be approximately independent of the grain size D whereas σ_{mc} depends on D. This dependence can be derived assuming that microcracking starts from some defects (e.g. small pores at the triple points of the polycrystalline structure), the size, say $2a$, of them being proportional to D. Then the Griffith criterion for a penny shaped flaw yields

$$\sigma_{mc} = \left(\frac{\pi E \gamma_{gb}}{2a}\right)^{1/2} = \frac{A}{D^{1/2}}, \quad (19)$$

where γ_{gb} is the specific fracture energy of a grain boundary. The new constant A comprises all parameters except the grain size D. An identical relation between σ_{mc} and D has been derived by Lange [15] using a more profound model for microcrack formation. Finally we must choose an appropriate value for n representing that dissipation zone size which must be exceeded in order that the energy dissipative process does increase the toughness. In this paper we assume that the diameter $2r_D$ of the zone at the transition point is about $2D$, this means $n = 1$. Using this result and Equations 18 and 19 we obtain from Equation 2

$$K_I^D = 3^{1/2}(A - \sigma_i D^{1/2}). \quad (20)$$

Thus we have derived K_I^D dependent on the grain size, the residual stress σ_i, and the grain boundary fracture energy included in A. The theoretical results, i.e. Equations 13, 15, 16, 17, and 20 will form the basis of our discussion in Section 4.

3. Experimental details

Dense polycrystalline single phase alumina specimens with about 5 mm x 5 mm cross-section were fabricated by cold pressing and sintering in H_2. At a constant average grain size of about 3 μm it turned out that the mechanical properties strongly depend on the actual kind of the grain size distribution [16]: Samples having two separate maxima of the distribution ($\bar{D}_1 = 2.1\,\mu$m, $\bar{D}_2 = 10$ to 15 μm) in the ideal case showed an improved strength of 500 to 600 MPa and $K_{Ic} = 7$ to 8 MPa $m^{1/2}$. Presumably this effect is due to microcracking preferentially starting around the larger grains and optimized with respect to microcrack length and density by the fine-grained matrix which hinders microcrack coalescence. For the present investigations underfired specimens with a lower fraction of larger grains and lower values of K_{Ic} were produced. They have been compared with samples made in an analogous manner and having the same average grain size (cf. Table I) but with a narrow monodisperse distribution instead of a bidisperse one.

To examine subcritical crack propagation the fracture induced photon emission was measured during 3-point-bending fracture in a high-vacuum chamber. The emission is generated at the crack tip by stress activated luminescence from a priori present point defects of the lattice. Details have been reported in a previous paper [17]. Due to the limited counting capacity of the electronics there

TABLE I Structure and properties of homogeneous (A) and bidisperse (B) aluminas. ρ denotes the microcrack density, σ_f the average fracture strength as measured directly in the course of the luminescence tests. K_I^* and K_{Ic} are the stress intensities for the macroscopically observable onset of subcritical crack growth and for instability, respectively. $I_c(B)/I_c(A)$ gives the ratio of cumulative photon emissions registered during bending fracture of specimens (A) and (B). VH is Vickers hardness measured at 98.1 N.

Grain structure	ρ	σ_f (MPa)	K_I^* (MPa $m^{1/2}$)	K_{Ic} (MPa $m^{1/2}$)	$I_c(B)/I_c(A)$
(A) $\bar{D} = 3.0\,\mu m$	1.4	305 ± 80	2.9 ± 0.3	5.0 ± 0.2	0.05–0.30 at VH = 16.4–17.8 GPa
(B) $\bar{D}_1 = 2.1\,\mu m$ (75 vol%) $\bar{D}_2 = 10$–$15\,\mu m$ (25 vol%) $\bar{D} \approx 3\,\mu m$ (all grains)	1.0	480 ± 60	4.6 ± 0.3	5.4 ± 0.2	

was only negligible contribution from the high-speed crack propagation at $K_I > K_{Ic}$ to the cumulative emission registered by a photomultiplier. Thus the emission I_c is a measure of the total amount of all subcritical crack growth processes. Comparing the two structures we found a systematic variation of $I_c(B)/I_c(A)$ with increasing hardness (cf. [17]); in Table I this is reflected by the stated range of data for $I_c(B)/I_c(A)$.

The critical stress intensity K_{Ic} has been determined by the usual notched beam test, by fractographic means from the Griffith equation using the fracture strength σ_f and the crack length C_f at final instability, and by indentation analysis. Besides K_{Ic} we have determined that value K_I^* where the subcritical crack growth becomes very rapid (10 to 100 $\mu m\,sec^{-1}$) and measurable crack extension can be observed. Testing the specimens with a usual loading rate (cross-head speed 0.5 mm min^{-1} at a span length of 30 mm), further increase of K_I up to K_{Ic} occurs primarily by quick subcritical crack growth at almost constant load. Therefore, the stress intensity K_I^* requested for the onset of quick subcritical crack propagation can be estimated combining σ_f with the flaw size C_0. This original flaw size C_0 and the subcritical crack growth boundary C_f have been determined on fractographs using a procedure very similar to that described by Kirchner and Gruver [18, 19]. Typically we have found $C_0 \approx 50\,\mu m$ and $C_f \approx 100$ to 200 μm.

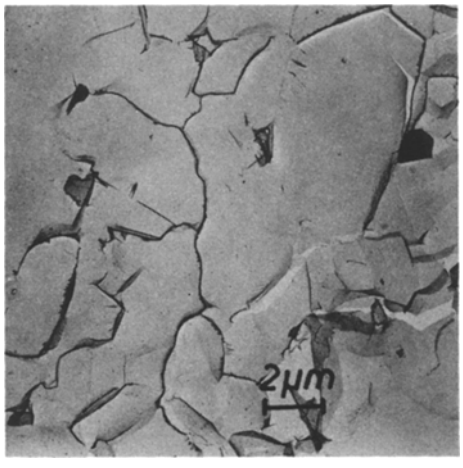

Figure 2 Microcrack system observed on a fracture surface of alumina. TEM micrograph; C–Pt-replica technique marks microcracks by dark contours following cracked grain boundaries.

In order to characterize the microprocess of energy dissipation the microcrack density ρ has been estimated from the lengths of microcrack traces measured on the fracture surface (replica micrographs) [16]. Fig. 2 presents an example of microcracking starting at a larger grain in a somewhat overfired bidisperse structure. The sum of the squares of the trace lengths related to the analysed surface area gives relative values for ρ as stated in Table I. Due to the special definition used such relative values can exceed unity. $\rho = 1.0$ for the underfired bidisperse samples was estimated from $\rho = 1.16$ as measured for the fully developed structure with $K_{Ic} = 7$ to 8 MPa $m^{1/2}$ [16]. Relating the microcracked area to the grain boundary area we obtained absolute crack densities of about 0.40.

4. Discussion

Table I shows markedly different amounts of luminescence emission I_c for the two ceramic structures. This fact may be explained by the occurrence of different modes of crack propagation. In order to verify this we must evaluate the conditions 15 to 17. To this end we first have to estimate the basic parameters appearing in the derived relations. Fracture starts within a structure which is thought as having no microcracks. First intensive spalling of grains at the tip of the macrocrack (the fracture initiating flaw) will occur at K_{Ic}^0, i.e. if K_I equals K_{Ic} of the most easily spalling

TABLE II Estimation of parameters used in the theoretical model for single phase polycrystalline alumina

Basic parameters	Parameters derived from Equation No.	
$\gamma\{\bar{1}012;\bar{1}010\} = 6$–$7\,\mathrm{J\,m^{-2}}$ [20]	$K_{Ic}^0 = 2.7\,\mathrm{MPa\,m^{1/2}}$	(4)
$\gamma_{gb} \approx \frac{1}{10}\gamma\{\bar{1}012\} \approx 0.6\,\mathrm{J\,m^{-2}}$	$A = 2.34\,\mathrm{MPa\,m^{1/2}}$	(19)
$E = 400\,\mathrm{GPa}$		
$2a \approx (0.1 \text{ to } 0.2)D$		
$\sigma_i \approx 150\,\mathrm{MPa}$ [21]		
$D = \begin{cases} 4\,\mu\mathrm{m}\ (\mathrm{A}) \\ 20\,\mu\mathrm{m}\ (\mathrm{B}) \end{cases}$	$K_I^D = \begin{cases} 3.5\,\mathrm{MPa\,m^{1/2}}\ (\mathrm{A}) \\ 2.9\,\mathrm{MPa\,m^{1/2}}\ (\mathrm{B}) \end{cases}$	(20) (20)

lattice planes of the Al_2O_3-crystal. Following Wiederhorn [20] this is about 2.1 to 2.5 $\mathrm{MPa\,m^{1/2}}$ for $\{\bar{1}012\}$ and $\{\bar{1}010\}$. Since the average orientation of such planes in a fracturing polycrystalline specimen will deviate from that of the macrocrack plane, a slightly higher value may be requested for K_{Ic}^0 (Table II). Once started, the crack accelerates and can proceed on grain boundaries providing an increased percentage of intercrystalline fracture as it has been observed by Kirchner and Gruver on fracture surfaces of sintered [18] and hot pressed [19] aluminas at $K_I \approx 3\,\mathrm{MPa\,m^{1/2}}$, which is only slightly beyond our estimation of K_{Ic}^0.

Furthermore, Table II presents the estimated values for the residual stress σ_i, for the microflaw size $2a$, for the grain boundary fracture energy γ_{gb} and the resulting constant A, which determines the critical stress for microcracking. Finally we must choose a characteristic value for D describing the size of those grains at which microcracking first occurs. Of course, the probability to find a grain of this size at the crack front must not be too low in order that a microcracked zone is really developed. Therefore K_I^D will be governed by a certain D between the average and the maximum diameter occurring in the grain size distribution.

Now we are in a position to apply the conditions 15 to 17 to our special alumina structures. The parameters K_{Ic}^0 and K_I^D may be obtained from Table II and K_{Ic}^1 is given by the macroscopic K_{Ic} (Table I).

(a) Homogeneous structure: $K_{Ic}^0 = 2.7\,\mathrm{MPa\,m^{1/2}}$, $K_I^* = 2.9\,\mathrm{MPa\,m^{1/2}}$, $K_I^D = 3.5\,\mathrm{MPa\,m^{1/2}}$, $K_{Ic}^1 = 5.0\,\mathrm{MPa\,m^{1/2}}$. For this structure the experimentally observed K_I^* practically equals K_{Ic}^0 whereas the threshold value K_I^D is well above K_{Ic}^0 and K_I^*. Inspection of condition 16 shows that crack propagation proceeds according to mode (ii). The initially moving crack is stopped at $C_s = 1.59\,C_0$ (Equation 13) after having reached C_D. Then again slow subcritial crack growth takes place and the applied load may be raised until K_{Ic} is reached.

(b) Bidisperse structure: $K_{Ic}^0 = 2.7\,\mathrm{MPa\,m^{1/2}}$, $K_I^D = 2.9\,\mathrm{MPa\,m^{1/2}}$, $K_I^* = 4.6\,\mathrm{MPa\,m^{1/2}}$, $K_{Ic}^1 = 5.4\,\mathrm{MPa\,m^{1/2}}$. Since the threshold value K_I^D is approximately equal to K_{Ic}^0 and well below K_I^* (describing the onset of quick subcritical crack growth), we conclude that energy dissipation has commenced already before the beginning of crack extension. This means that condition 15 applies and crack propagation proceeds according to mode (i).

Thus we now understand the considerably higher value of K_I^* for the bidisperse structure. Due to this K_I^* the outer boundary of the microcracked zone increases up to 50 to 70 μm already in the subcritical range (Equations 1, 18, and 19 using the maximum $D \approx 20$ to 25 μm). This r_D agrees well with our *in situ* observations made by means of a scanning electron microscope. Obviously in this case we must expect that microcracking occurs also around smaller grains situated in the central part of the dissipation zone. Therefore the microcrack density is thought to decrease with increasing distance from the microcrack tip. Although this may cause an additional influence onto the crack propagation mode in the region $K_I^* \leqslant K_I < K_{Ic}$ we do not expect substantial changes.

To illustrate our discussion Fig. 3 schematically shows the different stages of crack propagation starting from a flaw size assumed as 50 μm for both structures. The intermediate crack lengths were calculated from Equations 10 and 13. Dissipation zone sizes were obtained using Equations 1, 18, and 19 with the average grain size $\bar{D} = 3\,\mu$m for both structures (cf. Table I); thus the depicted zones represent a certain effective size between a minimum value belonging to the smaller grains and the outer boundary determined by the larger grains. The same effective zone size will be used for the estimation of luminescence.

Although the homogeneous structure exhibits

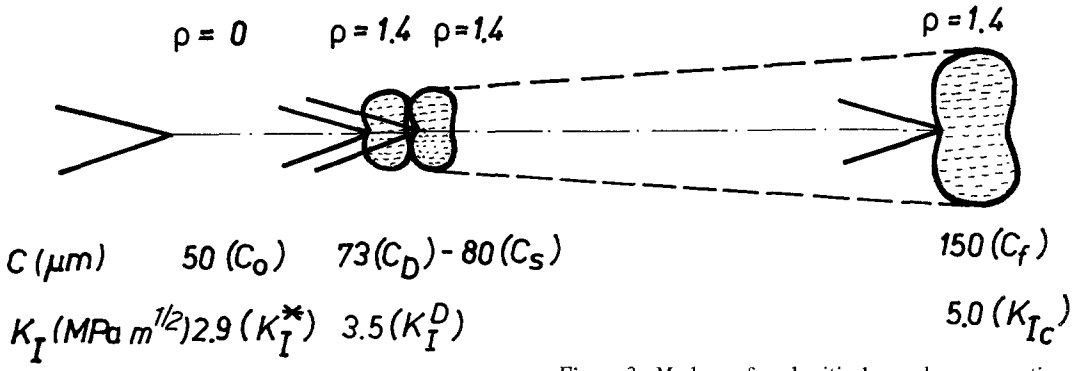

Figure 3 Modes of subcritical crack propagation in alumina structures with homogeneous and bidisperse grain size distribution, respectively.

a higher microcrack density ρ than the bidisperse one, the critical stress intensity factor K_{Ic} is lower. This can be understood since beyond a certain limit of the density ρ the microcracks tend to coalesce thereby reducing the toughness. However, a detailed discussion of K_{Ic} as dependent on ρ is not the aim of the present paper. Rather we would like to find out, whether our measurements of luminescence support the concept of different modes of crack extension as shown in Fig. 3. To this end we shall theoretically estimate the luminescence I_c to be expected for the two structures. According to the experimental technique, the cumulative emission I_c is proportional to the density of microcracks ρ and the area over which the microcracked zone moves during the subcritical stages of crack propagation:

$$I_c \sim \rho \int_{C_1}^{C_2} r_D(C)\mathrm{d}C, \qquad (21)$$

where C_1 and C_2 bound the region of subcritical crack growth. The density ρ in Equation 21 characterizes the average amount of microcracking exhibited by the different structures. In this sense we assume that ρ is almost constant in the subcritical stage of crack propagation, In addition we presuppose that only one macrocrack is initiated by the worst flow. For the size r_D of the microcracked zone we again have to use a certain average value since luminescence is a measure of the total amount of microcracking around the grains of all sizes concerned. Therefore we make use of Equation 1 assuming an effective critical stress σ_c determined by the average grain size $\bar{D}$ (cf. the above discussion to Fig. 3). Since $\bar{D}$ is identical for the two structures (Table I) we obtain from Equation 1 $r_D \sim K_I^2$, and Equation 21 may be rewritten as

$$I_c \sim \rho \int_{C_1}^{C_2} K_I^2(C)\mathrm{d}C. \qquad (22)$$

Because K_I^2 is a linear function of C (Equation 7), it can easily be shown that this integral is given by

$$I_c \sim \tfrac{1}{2}\rho(K_I^2(C_1) + K_I^2(C_2))(C_2 - C_1). \qquad (23)$$

The lengths C_1 and C_2 and the corresponding values for K_I can be taken from Fig. 3. For the homogeneous structure we have $C_1 = 73\,\mu m$ and $C_2 = 150\,\mu m$, whereas the behaviour of the bidisperse structure is described by $C_1 = 50\,\mu m$ and $C_2 = 70\,\mu m$. Using these data we obtain for the ratio of emission intensities $I_c(B)/I_c(A) = 0.25$. This result agrees fairly well with the experimentally observed emissions and seems to confirm our notion about different crack propagation modes. In addition, the correspondence between theory and experiment substantiates the assumption about the active role of microcracking in the

subcritical stage of fracture. This is also in accordance with the results of acoustic emission experiments, which indicated the formation of a microcracked zone before the onset of subcritical crack growth [22] and a dependence of such crack extension on the actual grain size distribution in sintered alumina [3, 23].

Nevertheless there are still some open problems. These concern especially the determination of the microcrack density, since only a two-dimensional section of the real three-dimensional network of cracks was examined. Moreover, only a certain average density independent of the actual propagation stage was measured. Also the determination of luminescence involved some difficulties since only microcracking on the sample surface contributes to the observed intensity. But one may hope that errors due to these problems are partially ruled out since we have considered only relative values of luminescence. Another problem is the following. The formation of the dissipation zone, especially in the bidisperse structure, is not such a step-like process as assumed by the theory. Hence a more detailed investigation taking into account the inhomogeneous structure of the microcracked zone seems to be useful in order to further understand the processes on the microscale.

6. Conclusions

A model has been presented for the initiation of energy-dissipative mechanisms in brittle materials. Energy is dissipated if the stress intensity at the tip of the macrocrack reaches a threshold value K_I^D. This can result in a new stabilization of the running crack if some conditions are met concerning the ratio between K_I^D and the two toughness levels K_{Ic}^0 (without energy dissipation) and K_{Ic}^1 (generated by the dissipative process). This model holds independently of the actual process of dissipation.

Experimental results obtained by measuring the fracture induced photon emission are readily explained if the theoretical model is combined with the idae of microcracking as the governing energy-dissipative mechanism in single phase sintered alumina. It turned out that the grain size distribution of the material plays an important role since the threshold stress intensity and the fracture toughness depend on it. Finally one may conclude that microcracking appears to be the dominating mechanism being responsible for the observed pecularities of crack propagation and for the mechanical properties of alumina structures.

Acknowledgements

The authors wish to express their gratitude to Professor W. Pompe and Professor D. Schulze for their interest in this work and the many helpful discussions.

References

1. R. W. RICE, S. W. FREIMAN and J. J. MECHOLSKY JR, *J. Amer. Ceram. Soc.* **63** (1980) 129.
2. R. W. RICE, R. C. POHANKA and W. J. MCDONOUGH, *ibid.* **63** (1980) 703.
3. B. J. DALGLEISH, P. L. PRATT, R. D. RAWLINGS and A. FAKHR, *Mater. Sci. Eng.* **45** (1980) 9.
4. J. P. SINGH, A. V. VIRKAR, D. K. SHETTY and R. S. GORDON, *J. Amer. Ceram. Soc.* **62** (1979) 179.
5. H. P. KIRCHNER and J. M. RAGOSTA, *ibid.* **63** (1980) 490.
6. A. V. VIRKAR, D. K. SHETTY and A. G. EVANS, *ibid.* **64** (1981) C–56.
7. W. POMPE, H. A. BAHR and W. KREHER, Proceedings of the 5th Symposium "Verformung und Bruch", Magdeburg, GDR, September 1979 (Technische Hochschule, Magdeburg, 1979) p. 33.
8. W. POMPE and W. KREHER, Proceedings of the 7th International Conference on Powder Metallurgy, Dresden, GDR, September 1981, Vol. 3 (Zentralinstitut für Festkörperphysik und Werkstofforschung, Dresden, 1981) p. 79.
9. T. K. GUPTA, F. F. LANGE and J. H. BECHTOLD, *J. Mater. Sci.* **13** (1978) 1464.
10. F. F. LANGE, ICM 1979, "Mechanical Behaviour of Materials" Vol. 3, edited by K. J. Miller and R. F. Smith (Pergamon Press, Toronto, 1979) p. 27.
11. N. CLAUSSEN, *J. Amer. Ceram. Soc.* **59** (1976) 49.
12. R. G. HOAGLAND, J. D. EMBURY and D. J. GREEN, *Scripta Metall.* **9** (1975) 907.
13. W. KREHER and W. POMPE, *J. Mater, Sci,* **16** (1981) 694.
14. R. G. HOAGLAND and J. D. EMBURY, *J. Amer. Ceram. Soc.* **63** (1980) 404.
15. F. F. LANGE, "Fracture Mechanics of Ceramics" Vol. 2, edited by R.C. Bradt, D. P. H. Hasselman and F. F. Lange (Plenum Press, New York, 1974) p. 599.
16. A. KRELL, *Phys. Stat. Sol. (a)* **63** (1981) 183.
17. *Idem, J. Mater. Sci.* **17** (1982) 1649.
18. H. P. KIRCHNER and R. M. GRUVER, *J. Amer. Ceram. Soc.* **63** (1980) 169.
19. *Idem. J. Mater. Sci.* **14** (1979) 2110.
20. S. M. WIEDERHORN, *J. Amer. Ceram. Soc.* **52** (1969) 485.
21. A. KRELL, PhD thesis, Academy of Science of the GDR 1981.
22. K. KŘÍŽ and F. W. KLEINLEIN, *Ber. Dt. Keram. Ges.* **57** (1980) 22.
23. B. J. DALGLEISH, A. FAKHR, P. L. PRATT *and* R. D. RAWLINGS, *J. Mater, Sci.* **14**(1979) 2605.

Received 12 May
and accepted 13 September 1982